Buckling in Armored Droplets
Electronic Supporting Information

François Sicard* and Alberto Striolo
Department of Chemical Engineering, University College London, Torrington Place, London WC1E 7JE, United Kingdom, EU

MD SIMULATION METHOD

The Dissipative Particle Dynamics (DPD) simulation method [1] was implemented within the simulation package LAMMPS [2]. The procedure and the parametrisation details are fully described in prior work [3, 4]. The system simulated here is composed of water, oil (decane), and nanoparticles (NPs). One "water bead" (w) represents 5 water molecules and a reduced density of one DPD bead is set to $\rho = 3$. One decane molecule is modeled as two "oil beads" (o) connected by one harmonic spring of length 0.72 R_c and spring constant 350 k_BT/R_c [5], where R_c is the DPD cutoff distance. The initial size of the simulation box is $L_x \times L_y \times L_z \equiv 72 \times 72 \times 78\ R_c^3$, where L_i is the box length along the i^{th} direction. Periodic boundary conditions are applied in all three directions. The NPs are modelled as hollow rigid spheres and contain polar (p) and nonpolar (ap) DPD beads on their surface. One DPD bead was placed at the NP center for convenience, as described elsewhere [3, 4]. Hollow models have been used in the literature to simulate NPs, and hollow NPs can also be synthesized experimentally [6]. We considered spherical NP of the same volume, $4/3\pi a_0^3$, where a_0 is the radius of the sphere. We imposed $a_0 = 2R_c \approx 1.5$ nm. All types of beads in our simulations have reduced mass of 1. We maintain the surface bead density on the NPs sufficiently high to prevent other DPD beads (either decane or water) from penetrating the NPs (which would be unphysical), as it has already been explained elsewhere [4]. To differenciate every NPs, we report the nonpolar fraction of the NP surface beads and the NP type. For example, $75HP$ ($55JP$) indicates that 75% (55%) of the beads on the NP surface are nonpolar, and that we consider an homogeneous (Janus) NP.

The interaction parameters shown in Table I are used here. These parameters were adjusted to reproduce selected atomistic simulation results, as explained in prior work [3]. By tuning the interaction parameters between polar or nonpolar NP beads and the water and decane beads present in our system, it is possible to quantify the effect of surface chemistry on the structure and dynamics of NPs at water-oil interfaces. Specifically, the interaction parameters between NP polar and nonpolar beads were adjusted to ensure that NPs are able to assemble and disassemble without yielding permanent dimers at the water/oil interface [3]. All simulations were carried out in the NVE ensemble [3]. The scaled temperature was 1, equivalent to 298.73 K. The DPD time scale can be gauged by matching the self-diffusion of water. As demonstrated by Groot and Rabone [5], the time constant of the simulation can be calculated as $\tau = \frac{N_m D_{\text{sim}} R_c^2}{D_{\text{water}}}$, where τ is the DPD time constant, D_{sim} is the simulated water self-diffusion coefficient, and D_{water} is the experimental water self-diffusion coefficient. When $a_{w-w} = 131.5\ k_BT/R_c$ (cf. Tab. I), we obtained $D_{\text{sim}} = 0.0063\ R_c^2/\tau$. For $D_{\text{water}} = 2.43 \times 10^{-3}\ cm^2/s$ [7], we finally obtain $\tau = 7.6$ ps.

TABLE I. DPD interaction parameters expressed in k_BT/R_c units. Symbols w, o, ap, and p stand for water beads, oil beads, NP nonpolar beads, and NP polar beads, respectively.

	w	o	ap	p
w	131.5	198.5	178.5	110
o		131.5	161.5	218.5
ap			450	670
p				450

While the traditional DPD algorithm can mimic hydrodynamics properties of the system [1], it cannot reproduce the vapour-liquid coexistence of water at the droplet interface [8]. This is due to the DPD conservative force, which determines the thermodynamics of the DPD system [1]:

$$\mathbf{F}_{ij}^C = \begin{cases} a_{ij}(1 - r_{ij}/R_c)\hat{\mathbf{r}}_{ij} & (r_{ij} < R_c) \\ 0 & (r_{ij} \geq R_c) \end{cases} \tag{S1}$$

where a_{ij} is the maximum repulsion strength between beads i and j introduced previously, $\mathbf{r}_{ij} = \mathbf{r}_i - \mathbf{r}_j$, $r_{ij} =\mid \mathbf{r}_{ij} \mid$, $\hat{\mathbf{r}}_{ij} = \mathbf{r}_{ij}/r_{ij}$, $\mathbf{r}_i$ and $\mathbf{r}_j$ are the positions of bead i and bead j, respectively. The DPD conservative force in Eq. (S1) yields an equation of state (EOS) [1]

$$p = \rho k_B T + \alpha a \rho^2 \ , \tag{S2}$$

where p is the pressure, ρ is the number density of the DPD beads, a is the repulsion strength, and α is a fitting parameter equal to 0.101 ± 0.001 in DPD reduced units [1]. As shown by Warren in Ref. [8], The DPD system is unstable for $a < 0$, so one is restrictided to $a \geq 0$ and therefore to strictly repulsive (conservative) interactions. This implies that calculations such as the vapor-liquid coexistence and free-surface simulations cannot be attempted. This can be adjusted by considering higher order terms of the density, ρ, in Eq. (S2), *i.e.* making the conservative force in Eq. (S1) density dependent [8].

SYSTEM CHARACTERISATION: DROPLETS AND NANOPARTICLES

In our simulations, the initial size of the droplet was fixed. At the beginning of each simulation, the solvent (oil) beads were distributed within the simulation box forming a cubic lattice. One water droplet of radius $\approx 20\ R_c$ was generated by replacing the oil beads with water beads within the volume of the spherical surface. A number of spherical NPs were placed randomly at the water-decane interface with their polar (nonpolar) part in the water (oil) phase to reach the desired water-decane interfacial area per NP. Following previous work [9, 10], the NPs considered in this study are spherical and of two different types: Janus and homogeneous. The emulsion systems are stabilized by a sufficiently dense layer of NPs [10]. We considered water droplets coated with 160 spherical Janus and homogeneous nanoparticles of type $55JP$ and $75HP$, respectively. Considering the NP surface coverage, ϕ, defined in Ref. [3], we obtain $\phi \approx 0.9$. Considering the results obtained in Ref. [3] for a flat interface, this yields an interfacial tension $\gamma_{ow} \approx 6.8\ k_B T/R_c^2$ for both Janus and homogeneous NPs. The initial configuration obtained was simulated for 10^6 timesteps in order to relax the density of the system and the contact angle of the nanoparticles on the droplet. The system pressure and the three-phase contact angles did not change notably after 5000 simulation steps. We let then run the system for an additional 2×10^6 timesteps to generate two new intial configurations after 2×10^6 and 3×10^6 timesteps, respectively. We then repeated the buckling simulation with these different initial configurations to test the reproducibility of the simulation.

The surface area of the droplets is *slowly* diminished, pumping randomly a constant proportion, *i.e.* 10 percent, of water molecules out of the droplet and letting the system pressure and the three-phase contact angles equilibrate at constant density. By *slowly*, we mean we do not create any hollow volume in the droplet that would strongly drive the system out-of-equilibrium. Doing so, the three-phase contact angle distribution of the NPs evolves sufficiently smoothly when the droplet buckles and becomes nonspherical, thereby preventing particles to be *artifactually* realeased. This numerical protocol can be similarly compared with an emulsion system where the dispersed phase is slightly soluble in the continuous phase [11]. By adding a fixed amount of unsatured continuous phase, the volume of the droplets can then be controllably reduced.

Three-phase contact angle. To estimate the three phase contact angle on the droplets we calculate the fraction of the spherical NP surface area that is wetted by water [12],

$$\theta_C = 180 - \arccos\left(1 - \frac{2A_w}{4\pi R^2}\right), \tag{S3}$$

where A_w is the area of the NP surface that is wetted by water and R is the radius of the NP. The ratio $A_w/4\pi R^2$ is obtained by dividing the number of NP surface beads (ap or p), which are wetted by water, by the total number of beads on the NP surface (192 for spherical NP). One surface bead is wet by water if a water bead is the solvent bead nearest to it. One standard deviation from the average is used to estimate the statistical uncertainty.

Radius of gyration. The description of the geometrical properties of complex systems by generalized parameters such as the radius of gyration or principal components of the gyration tensor has a long history in macromolecular chemistry and biophysics [10, 13, 14]. Indeed, such descriptors allow an evaluation of the overall shape of a system

and reveal its symmetry. Considering, e.g., the following definition for the gyration tensor,

$$\mathcal{T}_{GYR} = \frac{1}{N}\begin{bmatrix} \sum x_i^2 & \sum x_i y_i & \sum x_i z_i \\ \sum x_i y_i & \sum y_i^2 & \sum y_i z_i \\ \sum x_i z_i & \sum y_i z_i & \sum z_i^2 \end{bmatrix}, \tag{S4}$$

where the summation is performed over N atoms and the coordinates x, y, and z are related to the geometrical center of the atoms, one can define a reference frame where $\mathcal{T}_{GYR}$ can be diagonalized:

$$\mathcal{T}_{GYR}^{diag} = \begin{bmatrix} S_1^2 & 0 & 0 \\ 0 & S_2^2 & 0 \\ 0 & 0 & S_3^2 \end{bmatrix}. \tag{S5}$$

In this format we obey the convention of indexing the eigenvalues according to their magnitude. We thus define the radius of gyration $R_{GYR}^2 \equiv S_1^2 + S_2^2 + S_3^2$, and the asphericity $A_s \equiv S_1 - \frac{1}{2}(S_2 + S_3)$, which measures the deviation from the spherical symmetry. To determine the properties of a droplet, we calculate R_{GYR} and A_s using the centers of the water beads.

In this letter, Janus and homogeneous NPs present similar three-phase contact angle $\theta_c = (91.6 \pm 2.0)^\circ$ and $\theta_c = (88.7 \pm 3.5)^\circ$, respectively. The radius of gyration, R_{GYR}, and the asphericity, A_s, for the Janus and homogeneous initial configurations are $R_{\mathrm{GYR}} = 13.837 \pm 0.003$ and $R_{\mathrm{GYR}} = 13.860 \pm 0.003$, and $A_s = 0.156 \pm 0.05$ and $A_s = 0.153 \pm 0.05$, respectively, expressed in R_C units.

EVOLUTION OF THE NANOPARTICLE RADIAL DISTRIBUTION FUNCTION

The transition from dimples and cups to crater-like depression observed when Janus nanoparticles cover the droplet can be reflected in the temporal evolution of the radial distribution function of the NPs, $g(r)$, with r the distance between the centers of the NPs. We first consider the initial spherical configuration, and extract the list of nearest neighbours of each NP within a shell of radius $r < 12R_c$. This treshold value defines the first and second neighbouring shells [10, 15]. As the system is densely packed at the interface, we follow the temporal evolution of $g(r)$ considering this subset of particles, which corresponds to the nearest neighbours shell. When the volume of the droplet reduces, we first see in Fig. S1 (left panel) the emergence of a new peak around $r \approx 4.75R_C < r_{\mathrm{DPD}}$, where $r_{\mathrm{DPD}} = 5R_C$ represents the distance between the centers of NPs above which the NPs do not interact with each other through the DPD non-bonded force. As the droplet volume further reduces, the heigh of the new peak increases. This evolution continues until $\Delta N_W \approx 0.6$ (cf. Fig. 2 in the main text). Below that value, the heigh of the first peak decreases, together with the increase of the heigh of the second peak. This corresponds to the transition from dimples and cups to crater-like depression. The evolution continues until $\Delta N_W \approx 0.25$ where the number of water beads which remain in the droplet is not sufficient to define unambiguously the droplet volume.

As the $g(r)$ evolution between the homogeneous particles is concerned, we see in Fig. S1 (right panel), a constant increase of the heigh of the first peak, centered at $r \approx 4.75R_C$. This first peak located below r_{DPD} is already present in the initial spherical configuration, and is linked to the difference between the NP chemistry. Indeed, Janus NP are made of two hemispherical faces, one hydrophobic in contact with the hydrocarbon beads, and one hydrophilic in contact with the water beads. The NP hydrophobic faces which protrude in the solvent interact strongly and repeal each other to minimize the interaction potential energy. Unlike Janus NPs, both hemispherical faces of homogeneous NPs are made with hydrophobic and hydrophilic beads. This allows the NPs to interact smoothly with each other and to fluctuate more. Hence they can come closer than r_{DPD}, keeping spherical the droplet interface.

EVOLUTION OF THE THREE-PHASE CONTACT ANGLE DISTRIBUTION

In Fig. S2, we show the evolution of the three phase contact angle distribution of Janus (left panel) and homogeneous (right panel) NPs from the initial stage E_0 (cf. Fig. 1 in the main text), where the shape of the droplet is spherical, to the final stage E_{20}. The initial distributions, fitted with continuous lines, can be described with Gaussian distributions for both the Janus and homogenous emulsion systems. The values of the respective means, μ^J and μ^H,

and variances, σ^J and σ^H, differ according to the chemistry of the stabilizers. We obtain $\mu^J = 91.6°$ and $\mu^H = 88.6°$, and $\sigma^J = 2.0°$ and $\sigma^J = 3.4°$ for Janus and homogeneous NPs, respectively.

When the droplet is coated with Janus NPs, the system evolves to a skewed distribution as the droplet shrinks, but remains unimodal with a single peak at the same value as the one measured for the spherical initial configuration. The emergence of the skewness of the distribution is linked to the decrease of the NP-NP distance when the droplet volume is reduced due to the major role played by the steric effect. The evolution is different when homogeneous NPs cover the droplet. As the volume is reduced, the contact angle distribution firstly evolves as a monolayer interface with a single peak (from E_0 to E_5, Fig. 1 in the main text). As the distance between the NPs decreases further, the distribution becomes bimodal as two distinct peaks emerge on both sides of the original equilibrium contact angle. This fundamental difference is characteristic of a particle bilayer.

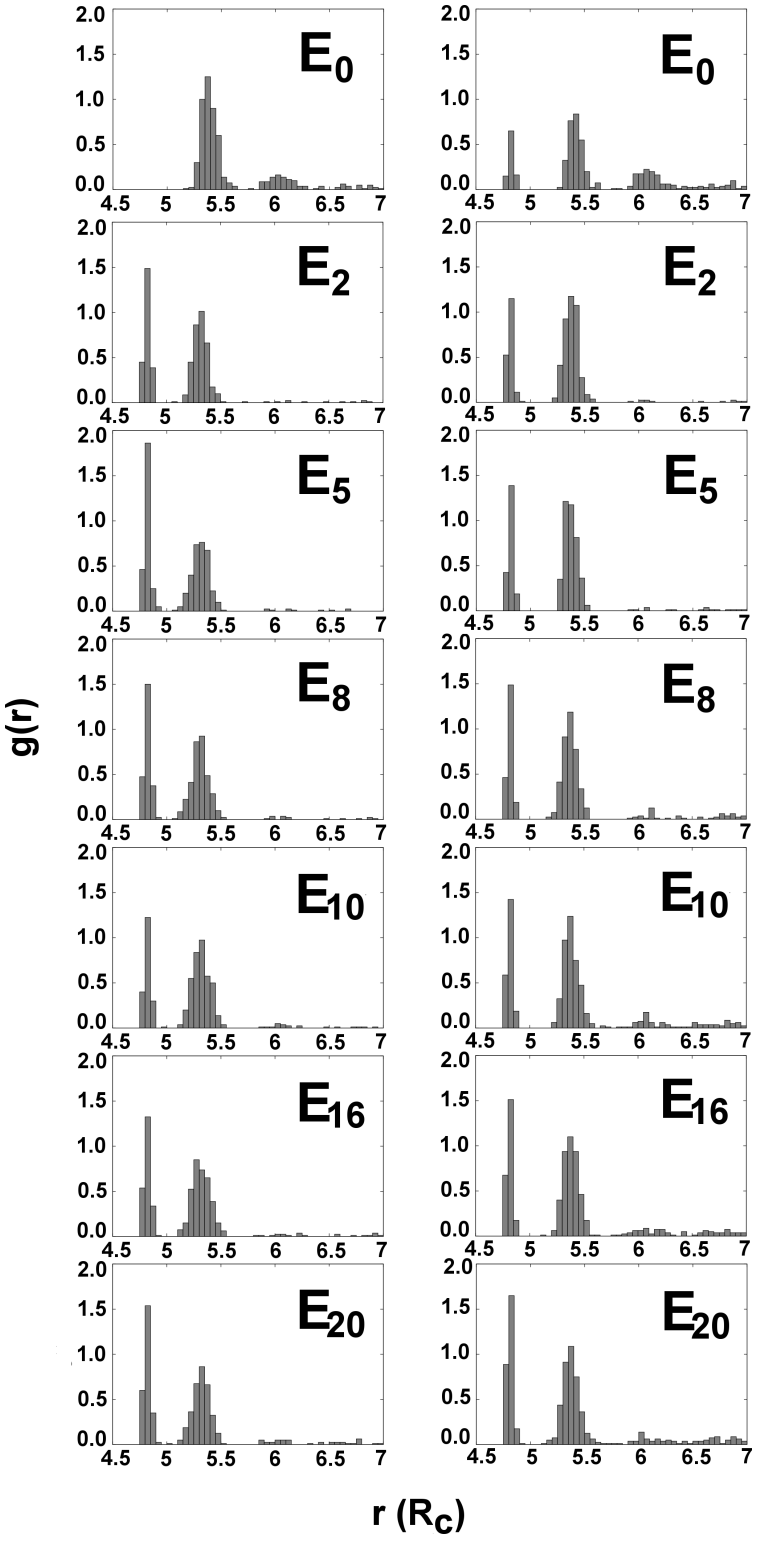

FIG. S1. Evolution of the radial distribution function of the NPs, $g(r)$. r is the distance between the centers of the NPs. The water droplet is coated with Janus (left) and homogeneous (right) particles. For comparison with snapshots in Fig. 1 in the main text, E_i refers to the i^{th} removal of water beads. We follow the evolution of the first and second neighbouring shells.

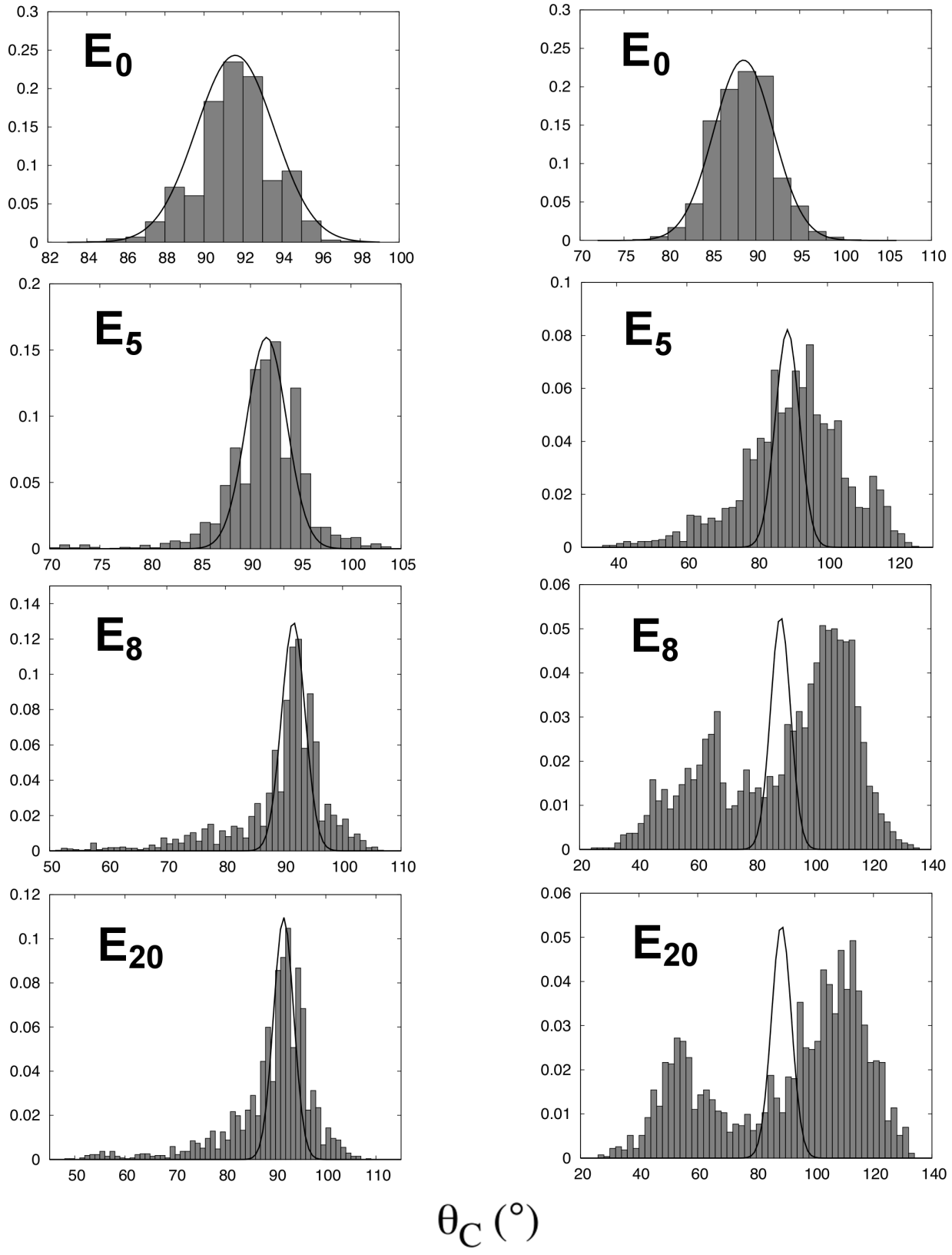

FIG. S2. Evolution of the three-phase contact angle distribution, θ_C, of Janus (left panels) and homogeneous (right panels) NPs. For comparison with snapshots in Fig. 1 in the main text, E_i refers to the i^{th} removal of water beads. The initial distributions (stage E_0) are fitted with Gaussian distributions, which are plotted at every stage, for comparison. For clarity, we rescale the height of the Gaussian distributions at every stage.

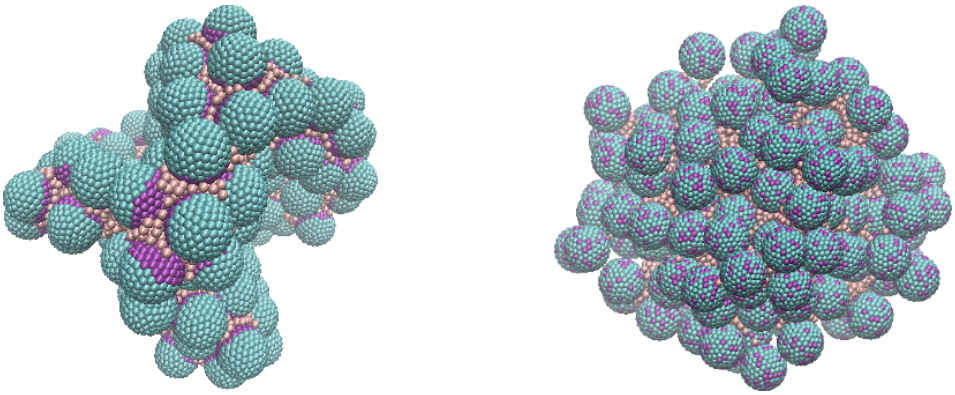

FIG. S3. Snapshots of the final configurations E_{20} of the buckling processes of water droplets armored with 160 spherical Janus (left) and homogeneous (right). The proportion of water beads removed is around 10 percent in each evaporation. The equilibration time after each evaporation is reduced to 2×10^3 timesteps (instead of 10^5 as in the main text).

HOW NUMERICAL ALGORITHMS AFFECT THE DROPLET EVOLUTION

In our mesoscopic analysis, we controllably reduced the volume of the droplet, removing a constant proportion, *i.e.* 10 percent, of water beads from the droplet. As a consequence, the three-phase contact angle distribution of the NPs evolves smoothly when the droplet buckles, thereby preventing particles to be artifactually released. However, the particles behaviour strongly depends on the numerical protocol.

In Fig. S3, we show qualitatively, for comparison, the evolution of the droplet volume when the equilibration time after each water bead removal is reduced. The proportion of water beads removed remains in 10 percent in each stage. When the droplet is coated with homogeneous NPs (right panel), we observe that the shape of the droplet remains spherical, with some NPs desorbed in the organic solvent. This evolution is representative of the *passive* role played by the homogeneous NPs and is in agreement with experiments [16]. When the droplet is coated with Janus NPs (left panel), we observe a significant curved-shape deformation of the droplet, along with the abscence of NP release. This evolution is representative of the *active* role played by the Janus NPs. The morphology of the droplet becomes noticeably crumpled, with large dimples, and no transition to crater-like depression is observed. This results are consistent with the *surface model* numerical analysis from Ref. [17], where more than one dimple may nucleate if the evaporation is *rapid*, leading to metastable multi-indented shapes. Experimentally, the term *rapid* may correspond to kinetic barriers, which prevent thermally activated coalescence between adjacent dimples. Our result highlights the central role played by the relaxation time of the system after each evaporation in the evolution of the interface geometry.

REFERENCES

[1] R. Groot and P. Warren, J. Chem. Phys. **107**, 4423 (1997).
[2] S. Plimpton, J. Comp. Phys. **117**, 1 (1995).
[3] X.-C. Luu, J. Yu, and A. Striolo, Langmuir **29**, 7221 (2013).
[4] X-C.Luu, J. Yu, and A. Striolo, J. Phys. Chem. B **117**, 13922 (2013).
[5] R. Groot and K. Rabone, Biophys. J. **81**, 725 (2001).
[6] M. Calvaresi, M. Dallavalle, and F. Zerbetto, Small **5**, 2191 (2009).
[7] J. Partington, R.F.Hudson, and K. Bagnall, Nature **169**, 583 (1952).
[8] P. Warren, Phys. Rev. E **68**, 066702 (2003).
[9] X.-C. Luu and A. Striolo, J. Phys. Chem. B **118**, 13737 (2014).
[10] F. Sicard and A. Striolo, Faraday Discuss. **191**, 287 (2016).
[11] S. Datta, H. Shum, and D. Weitz, Langmuir Lett. **26**, 18612 (2010).
[12] H. Fan and A. Striolo, Soft Matter **8**, 9533 (2012).
[13] J. Vymetal and J. Vondrasek, J. Phys. Chem. A **115**, 11455 (2011).
[14] K. Solc, J. Chem. Phys. **55**, 335 (1971).
[15] H. Fan and A. Striolo, Phys. Rev. E **86**, 05610 (2012).
[16] V. Garbin, J. Crocker, and J. Stebe, Langmuir **28**, 1663 (2012).
[17] C. Quilliet, Eur. Phys. J. E. **35**, 48 (2012).